DIRECT NUMERICAL SIMULATION OF NON-ISOTHERMAL TURBULENT WALL-JETS

Daniel Ahlman, Geert Brethouwer, Arne V. Johansson
Linné Flow Centre, Dept. of Mechanics,
Royal Institute of Technology
SE-100 44 Stockholm, Sweden
ahlman@mech.kth.se

ABSTRACT

Direct numerical simulations of plane turbulent non-isothermal wall-jets are performed and compared to the isothermal case. Two non-isothermal cases are studied; a cold jet propagating in a warm environment with inlet ambient to jet density ratio of $\rho/\rho_j = 0.4$, and a warm jet in a cold surrounding where $\rho_a/\rho_j = 1.7$ at the inlet. The ambient and wall temperature are kept equal and constant, and a temperature dependent viscosity is used. Results from the non-isothermal cases are compared to those obtained in a previously studied isothermal wall-jet with the same inlet Reynolds and Mach numbers. A passive scalar is also included in the simulations to study mixing. The influence of the varying temperature on the development and jet growth is studied as well as the influence on turbulence statistics and fluctuation intensities of the temperature and passive scalar. The warm jet contains smaller turbulent structures, and the cold jet larger, than the isothermal one. The change in structure and intensity affect the development and mixing in the jets.

INTRODUCTION

A plane wall-jet is obtained by injecting fluid along a solid wall such that the velocity of the jet supersedes that of the ambient flow. The structure of a developed turbulent wall-jet can formally be described as two adjacent shear layers of different character. The inner layer, reaching from the wall up to the maximum mean streamwise velocity, resembles a thin boundary layer, while the outer part, positioned above the inner layer and reaching out to the ambient flow, can be characterized as a free shear flow. As a consequence of this twofold nature, properties such as mixing and momentum transfer exhibit distinctively different character throughout the wall-jet.

Walls-jets are in practice often used for mixing and transport of scalars like heat and fuels. Examples of applications are in film cooling, ventilation and in separation control. Wall-jets are also of interest in combustion since combustion applications often include instances with mixing and reactions near walls. Results from wall-jets can be used to draw conclusions and increase the knowledge on how the wall affects mixing and reactions processes in the near wall region. Information from the present flow case, including effects of a varying density, are therefore of interest.

Numerous experimental investigations of the isothermal plane wall-jet have been performed. Experiments published prior to 1980 have been compiled and critically reviewed by Launder and Rodi (1981, 1983). More recently Eriksson et al. (1998) used LDV to perform accurate measurements of a $Re = 9600$ wall-jet. Their velocity measurements resolved also the viscous sublayer, enabling direct determination of the wall shear stress. Numerical studies of the plane wall-jet on the other hand are however scarce. Recently Dejoan and Leschziner (2005) performed a highly resolved LES, matching the experiments of Eriksson et al. (1998). In a following paper the wall influence was studied in an effort to separate the effects of wall blocking and near-wall shear (Dejoan and Leschziner, 2006). Ahlman et al. (2007) performed DNS to study the development and mixing in a plane wall-jet. Considering the wall-jet transition to turbulence, Levin et al. (2005) used linear analysis and DNS to study the laminar breakdown of a wall-jet.

Scalar mixing is of interest in a range of areas including e.g. atmospheric pollutant transport and combustion, and a number of studies have been devoted to mixing in generic flow cases. Stanley et al. (2002) used DNS to investigate mixing in a plane jet. Su et al. (2003) studied fine-scale scalar mixing in the same configuration using Rayleigh scattering and laser-induced fluorescence (LIF). Antoine et al. (2001) applied LIF and 2D laser Doppler velocimetry (LDV) to study mass transport and passive scalar mixing in a round jet with coflow. Mixing in a reacting environment has recently been studied by means of DNS in a reacting shear layer by Pantano et al. (2003) and in a reacting methane-air jet by Pantano (2004). The influence of density variations of turbulent flows with and without reactions are summarized in Fulachier et al. (1989).

In the present study, we analyze the development and statistics of plane non-isothermal turbulent wall-jets, by means of three-dimensional direct numerical simulations. Non-isothermal in this case implies that varying temperature and density inlet profiles are specified. Both the case of a cold jet in a warmer surrounding and a warm jet in a colder surrounding are simulated. Properties of the non-isothermal jets are compared to results obtained in an isothermal jet (Ahlman et al. 2007), using the same inlet Reynolds and Mach numbers in all simulations.

GOVERNING EQUATIONS

The governing equations in all jet simulations are the fully compressible Navier-Stokes equations

$$\frac{\partial \rho}{\partial t} + \frac{\partial \rho u_j}{\partial x_j} = 0 \tag{1}$$

$$\frac{\partial \rho u_i}{\partial t} + \frac{\partial \rho u_i u_j}{\partial x_j} = -\frac{\partial p}{\partial x_i} + \frac{\partial \tau_{ij}}{\partial x_j} \tag{2}$$

$$\frac{\partial \rho E}{\partial t} + \frac{\partial \rho E u_j}{\partial x_j} = \frac{\partial}{\partial x_j}\left(\lambda \frac{\partial T}{\partial x_j}\right) + \frac{\partial (u_i(\tau_{ij} - p\delta_{ij})}{\partial x_j} \tag{3}$$

where ρ is the mass density, u_j the velocity vector and $E = \rho(e + (u_i u_i)/2)$ the total energy. Fourier's law, where λ is the coefficient of thermal conductivity, has been used to approximate the energy fluxes. The stress tensor is defined

as

$$\tau_{ij} = \mu\left(\frac{\partial u_i}{\partial x_j} + \frac{\partial u_j}{\partial x_i}\right) - \frac{2}{3}\mu\delta_{ij}\frac{\partial u_k}{\partial x_k} \quad (4)$$

To also enable a study of the jet mixing, the compressible flow equations are supplemented with a transport equation for a passive scalar

$$\frac{\partial \rho\theta}{\partial t} + \frac{\partial}{\partial x_j}\left(\rho u_j \theta\right) = \frac{\partial}{\partial x_j}\left(\rho\mathcal{D}\frac{\partial \theta}{\partial x_j}\right) \quad (5)$$

The passive scalar equation is analogous to the mixture fraction equation commonly used in modelling of non-premixed combustion.

SIMULATION METHOD

The simulations are performed employing a sixth-order compact finite difference scheme (Lele, 1992) for the spatial discretization, and a third-order low-storage Runge-Kutta scheme for the temporal integration. In order to minimize reflections at in- and outlets, boundary zones as described by Freund (1997) are applied. The goal of the investigation is to study turbulent wall-jets, hence high magnitude disturbances ($u'_{rms} = 0.065U_{in}$) are applied at the inlet to facilitate a fast and efficient transition to turbulence. Three types of disturbances; random but correlated in time and space (Klein, 2003), streamwise vortices in the upper shear layer and harmonic forcing are superpositioned at the inlet. The simulation method is presented in more detail in Ahlman et al. (2007).

Table 1: Simulation cases.

Jet	ρ_a/ρ_j	Dimensions (h)	$N_x \times N_y \times N_z$
Isothermal	1.0	$47 \times 18 \times 9.6$	$384 \times 192 \times 128$
Cold	0.4	$35 \times 17 \times 7.2$	$384 \times 192 \times 160$
Warm	1.7	$28 \times 14 \times 7.2$	$448 \times 256 \times 160$

Table 2: Resolution in the turbulent part $x/h \geq 15$.

Jet	Δx^+	Δy_1^+	Δz^+
Isothermal	$10.7 - 11.8$	$0.86 - 1.3$	$5.5 - 8.2$
Cold	$3.0 - 3.1$	$0.29 - 0.37$	$1.3 - 1.7$
Warm	$12.5 - 12.9$	$1.2 - 1.5$	$7.5 - 9.5$

SIMULATION SETUP

The simulation domain is rectangular with a no-slip wall at the bottom. The inlet Reynolds number is $Re = U_{in}h/\nu = 2000$, where U_{in} is the the inlet jet velocity and h is the inlet jet height. The corresponding inlet Mach number used in the simulations is $M = U_{in}/c = 0.5$. The inlet Reynolds and Mach numbers are equal in all simulations. It should be noted that in the isothermal wall-jet, the compressibility effects where found to be negligible. Above the jet a slight coflow of $U_c = 0.10U_{in}$ is applied for computational efficiency reasons. Particularly at startup large scale vortices may develop above the jet. Using a coflow allows large persistent scales of this type to be convected out of the domain.

In the isothermal simulation the density and the energy profile at the inlet are constant. In the non-isothermal cases the inlet energy and density profiles are varied to generate a cold jet in a warm surrounding and correspondingly a warm jet in a cold environment. The non-isothermal cases are characterized by the ratio of ambient to jet density at the inlet $\alpha_\rho = \rho_a/\rho_{in}$. In the cold jet case an ambient density ratio of $\alpha_\rho = 0.4$ is used. The inlet jet temperature is defined to be $293K$ implying an ambient inlet temperature of $732.5K$. For the warm jet a ratio of 1.7 is used, the ambient temperature is set to $293K$ and hence an inlet jet temperature of $498.1K$. The temperature on the wall is kept constant and equal to the ambient condition. For the passive scalar a no-flux boundary condition is imposed, $(\partial\theta/\partial y)_{y=0} = 0$.

To account for the substantial variations in density and temperature in a natural way, a temperature dependent viscosity is used in the non-isothermal cases. The viscosity is determined by Sutherlands law

$$\frac{\mu}{\mu_J} = \left(\frac{T}{T_J}\right)^{3/2}\frac{T_J + S_0}{T + S_0} \quad (6)$$

where T is the local temperature and T_J the jet center temperature at the inlet. The reference coefficient used is $S_0 = 110.4K$, valid for air at moderate temperatures and pressures. As will be further discussed later, the cold and warm jet flow differ significantly in terms of the range of scales present, and hence different resolution and box sizes are used for the three cases. The simulation parameters and resolutions used in the three cases are summarized in table 1. The smallest scales in the jet are found close to the wall, coinciding with the energy dissipation maximum. Wall units are therefore used in table 2 to quantify the numerical resolution. Values in the region where the flow is turbulent, $x/h > 15$, are presented. The resolution for the isothermal and warm jets are comparable to what is typically used in channel flow simulations (see e.g. del Álamo, 2006). The resolution of the cold jet is significantly higher.

Concerning the transport properties of the passive and active scalar (heat), constant Schmidt and Prandtl numbers are assumed. For the scalar $Sc = \mu/\rho\mathcal{D} = 1$, implying that the diffusion term, $\rho\mathcal{D}$, has the same temperature dependence as the viscosity. The Prandtl number is $Pr = \mu c_p/\lambda = 0.72$ and a constant heat capacity is assumed implying that the heat conductivity also has the same temperature dependency.

JET DEVELOPMENT

The statistics of the turbulent jet development in the three cases is presented below. If not noted elsewise, all statistics shown are computed using Reynolds averaging.

To provide an overview of the jet structure in the simulated cold, isothermal, and warm jet, snapshots of the streamwise velocity are presented in figure 1. The flow structure is distinctly different in the three cases. The warm jet contains significantly smaller spatial scales than the other two. The structures in the isothermal jet are visibly larger, and the cold jet contains even larger typical scales. Evidently the temperature and density properties of the jets significantly influence the turbulent jet structure even though the inlet Reynolds is equal in all cases.

The inner part of the wall-jet closely resembles a zero-pressure gradient boundary layer (Ahlman et al., 2007). The conventional boundary layer scaling can therefore be applied to study properties of the inner shear layer. Mean streamwise velocity profiles are shown in figure 2 using boundary layer scaling in terms of $y^+ = y/l^* = yu_\tau/\nu_w$ and $U^+ = U/u_\tau$, where the friction velocity is defined as

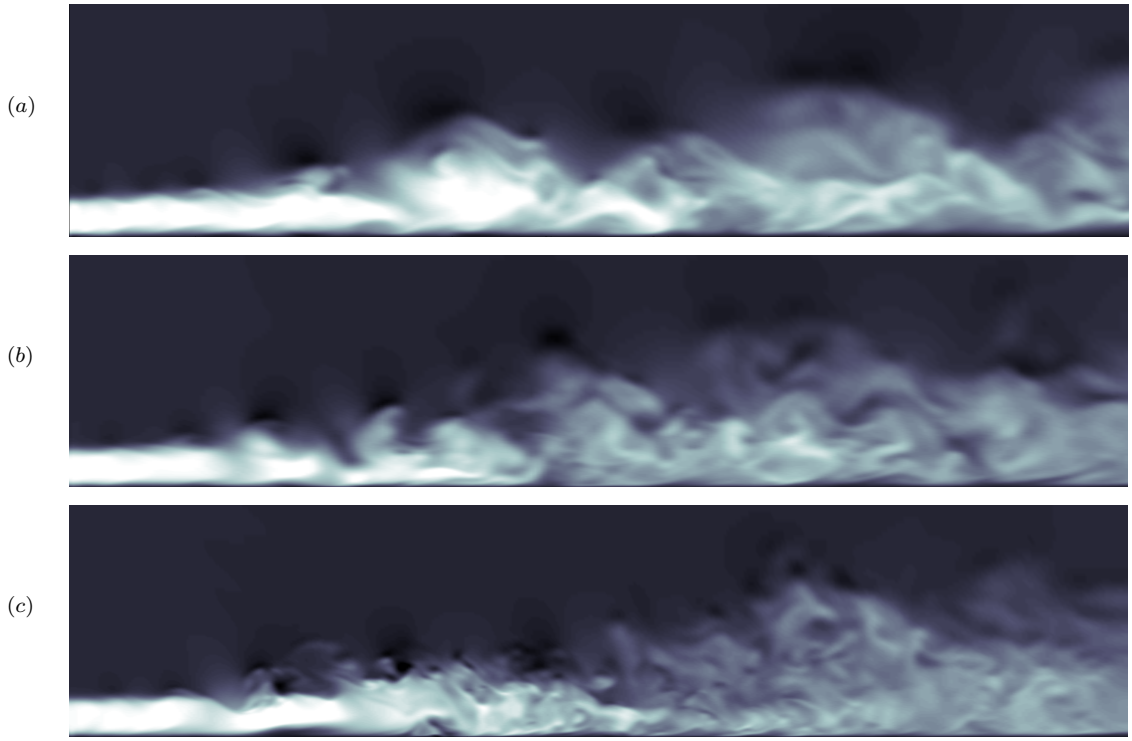

Figure 1: Snapshots of the streamwise velocity in the cold (a), isothermal (b) and warm jet (c).

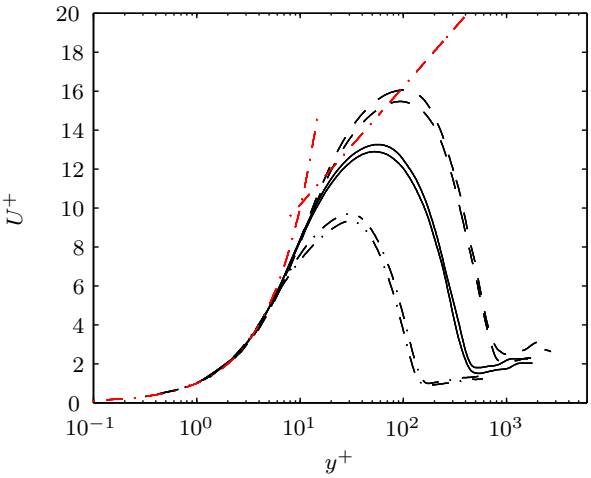

Figure 2: Mean streamwise velocity in inner scaling at downstream positions $x/h = 20$ and 25. Isothermal (solid), warm (dashed) and cold jet (dash-dotted) results. Viscous $U^+ = y^+$ and inertial sublayer $U^+ = \frac{1}{0.38}\log(y^+) + 4.1$ (Österlund et al. 2000) added.

$u_\tau = \sqrt{\tau_w/\rho_w}$ and the subscript w denotes wall conditions. The inner scaled profiles are markedly different for the three jets. Profiles in the warm jet attain higher values, and the profiles extend to higher y^+-values than the isothermal results, while cold jet profiles show the opposite behavior. The differences in the profiles indicate that the friction velocity u_τ and length scale l^* vary substantially in the simulated jets. An understanding of the origins of the differences can be obtained by examining the friction Reynolds number

$$Re_\tau = \frac{\delta}{l^*} = \frac{u_\tau \delta}{\nu_w} = \frac{\delta}{\nu_w^{1/2}} \sqrt{\left(\frac{dU}{dy}\right)_{y=0}} \qquad (7)$$

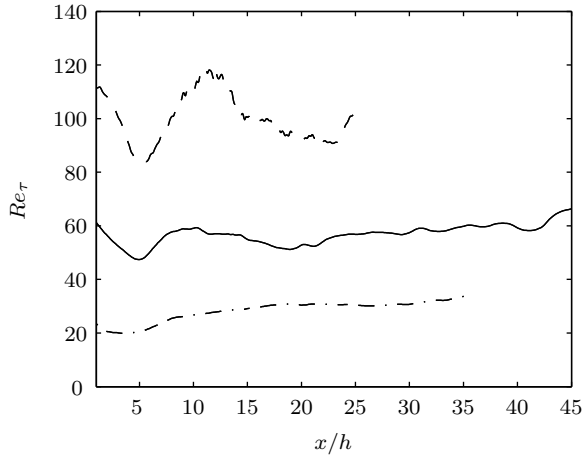

Figure 3: Friction based Reynolds number $Re_\tau = u_\tau y_m/\nu$. Isothermal (solid), warm (dashed) and cold jet (dash-dotted) results.

which, if an appropriate outer scale δ is applied, provides an estimate of the inner to outer scale ratio. In the warm jet the kinematic viscosity decreases towards the colder wall which tends to increase the friction Reynolds number. In the cold jet the warmer wall instead generates a higher viscosity and hence a reduced scale separation. The friction Reynolds number for the three jets, using the maximum streamwise velocity position y_m as outer scale, is shown in figure 3, where it is clear that the viscous to outer scale ratio is highest in the warm jet and lowest in the cold.

According to figure 2 all streamwise profiles collapse in the viscous sublayer, which also has the same approximate width, $y^+ \leq 5$, in the three cases. Further away from the wall, an inertial sublayer in correspondence to a boundary layer is assumed to exist and logarithmic overlap regions

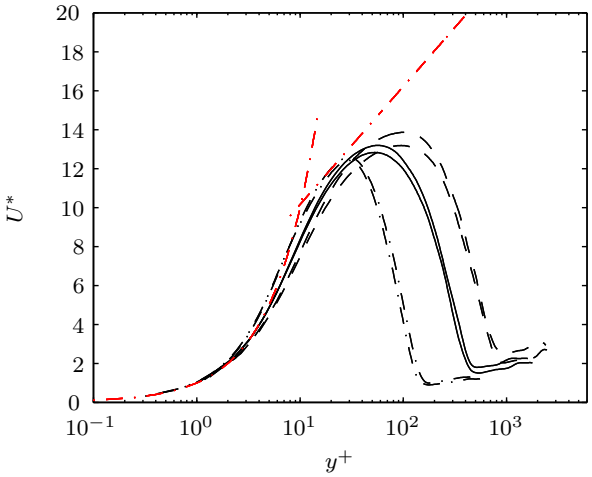

Figure 4: Density-weighted mean streamwise velocity in inner scaling at downstream positions $x/h = 20$ and 25. Isothermal (solid), warm (dashed) and cold jet (dash-dotted) results. Viscous and inertial sublayers as if figure 2 added.

have been found in experiments and large-eddy simulations at sufficiently high Reynolds numbers. No such region is however found in the present study, presumably because of the moderate Reynolds number used in the simulations. The absence of logarithmic overlap regions is also seen in the density-weighted profiles plotted in figure 4. Density-weighting is performed through $U^* = \sqrt{\bar{\rho}/\bar{\rho}_w}U^+$, where $\bar{\rho}$ is the local mean density, and $\bar{\rho}_w$ the corresponding wall density. The applied weighting brings the warm and cold profiles to isothermal values in the region prior to the maximum position, but still no logarithmic region is present. The collapse in the viscous region is also reduced by the density-weighting.

The mean jet development in the three cases is shown in figure 5-6, where the mean streamwise velocity and temperature are plotted scaled by inlet and ambient conditions respectively. The profiles shown are taken at downstream positions of $x/h = 20$ and 25, where the jets are fully turbulent. The mean velocity and temperature in the warm jet decay faster than in the other cases. Fast turbulent transport and mixing also produces steeper mean gradients near the wall and move the maxima and minima in velocity and temperature closer to the wall. The opposite effects occur in the cold jet.

The wall-jet growth is depicted in figure 7 in terms of the development of the half-width $y_{1/2}$, defined as the position in the outer shear layer where the velocity attains half the maximum excess value, i.e $U(y_{1/2}) = (U_m - U_c)/2)$. Incompressible wall-jets are known to experience a linear half-width growth, in correspondence to what is also found in self-similar free plane jets. The non-isothermal jets are also found to grow linearly when the flow is turbulent. The growth rate is however seen to be slightly influenced by the density variation. The cold jet grows somewhat faster and the warm jet slightly slower than the isothermal. This is in agreement with previous observations concerning the Reynolds dependence. It has been seen that the growth rate decreases with increasing Reynolds number (see e.g. Abrahamsson et al. 1994). In the non-isothermal jets the Reynolds numbers are equal but, as seen above, the inner to outer scale ratio is different and dependent on the wall temperature. A higher scale ratio exists in the warm jet which gives a lower growth rate in correspondence to a

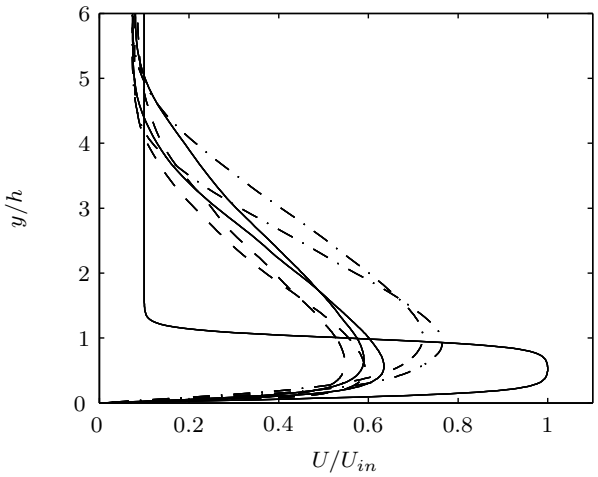

Figure 5: Mean velocity, normalized by jet inlet velocity, at downstream positions of $x/h = 20$, and $x/h = 25$. Isothermal (solid), warm (dashed), and cold (dash-dotted) jet profiles. Note that the inlet velocity profiles overlap.

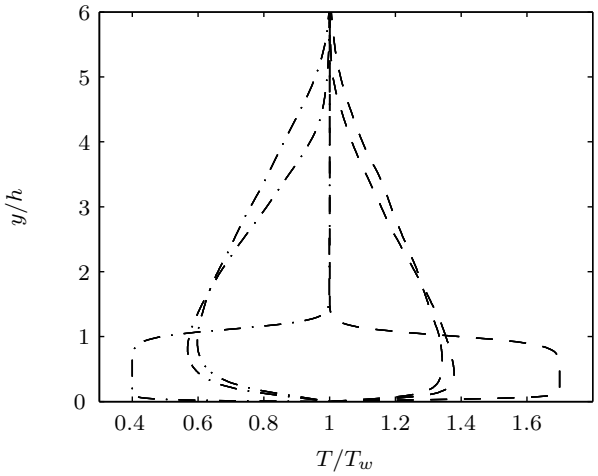

Figure 6: Mean temperature, normalized by the ambient temperature, at downstream positions of $x/h = 20$, and $x/h = 25$. Warm (dashed), and cold (dash-dotted) jet profiles.

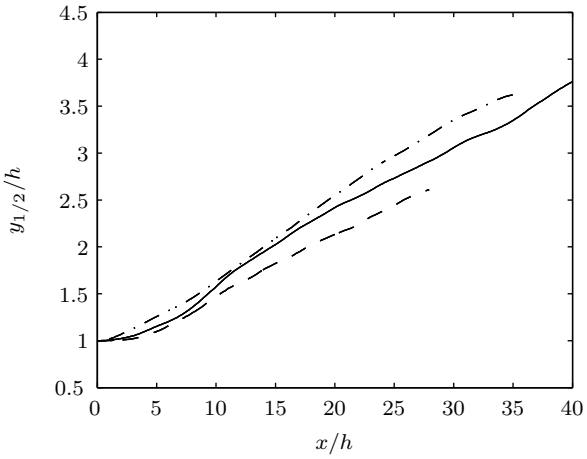

Figure 7: Growth of the jet half-width: isothermal (solid), warm (dashed), and cold jet (dash-dotted).

higher Reynolds number jet. Despite the differences in inner Reynolds number, the transition to turbulence and start of the linear growth, occur at approximately the same position, $x/h = 12$.

TURBULENCE STATISTICS

The wall-jet turbulent kinetic energy profiles using inner viscous scaling are presented in figure 8. Favre averaging is used for the isothermal profiles, which for this case is assumed to give practically identical results to Reynolds averaging. In the inner viscous sublayer, $y^+ \leq 5$, the profiles collapse, as was the case for the mean profiles. The turbulent energy outside the viscous sublayer is significantly influenced by the varying temperature. As for the mean velocity in figure 2 the warm profiles attain higher magnitudes, and extend to higher y^+-values compared to profiles of the isothermal jet, while the situation is opposite for the profiles of the cold jet. The influence of different scaling approaches, such as local density scaling (Huang et al., 1995), as well as the differences between Reynolds and Favre averaging needs to be further addressed for this flow case.

The Reynolds shear stress shown in figure 9 behaves in a manner corresponding to the kinetic energy, with increasing intensity when the jet temperature increases. The inner negative peak in the Reynolds stress increases in magnitude and moves further away from the wall. These tendencies are also found in channel flows, where the Reynolds shear stress magnitude in inner scaling tends to -1 for increasing Reynolds numbers (Österlund, 1999).

SCALAR FLUCTUATION INTENSITIES

The temperature and passive scalar fluctuation intensities are shown in figure 10 and 11, where both intensities are scaled by the respective mean properties at the wall. It should be noted that the temperature is an active scalar and affects the flow while this is not the case for the passive scalar. In the simulation different boundary conditions are also prescribed for the temperature and the passive scalar. The temperature is kept constant on the wall while a no-flux condition is used for the scalar. Observing the temperature fluctuation intensity, the fluctuations in the warm jet are found to extend further out from the wall in terms of the half-width. Also the difference between the intensity in the inner and outer shear layers is less pronounced in the warm jet. This is in unintuitive in the sense that in previous statistics the increased scale separation acted to pronounce differences in the inner and outer layers.

The passive scalar fluctuation intensity in the three jets is compared in figure 11. The mean concentration is not able to collapse the fluctuation in the inner region . In the near the half-width, the fluctuation intensity is approximately equal in the three jets. Further away from the wall the scalar fluctuation in the warm jet increases, a tendency that is not present in the other two cases.

CONCLUSIONS

Direct numerical simulation of two non-isothermal wall-jets have been performed and statistics of the jet development, turbulent properties, and mixing were presented. The results were compared to the situation in a isothermal jet at the same inlet Reynolds and Mach numbers, defined at the jet center. Despite the corresponding Reynolds number, the scale separation in the warm jet, in terms of the viscous to

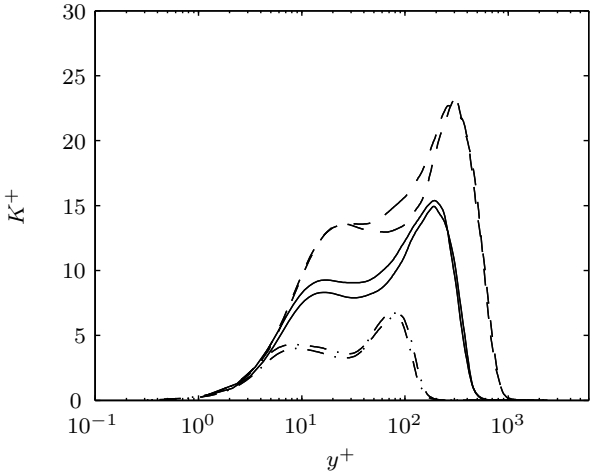

Figure 8: Turbulent kinetic energy in inner scaling at downstream positions $x/h = 20$ and 25. Isothermal (solid), warm (dashed) and cold jet (dash-dotted) results. Note that Favre averaging is used for the isothermal results.

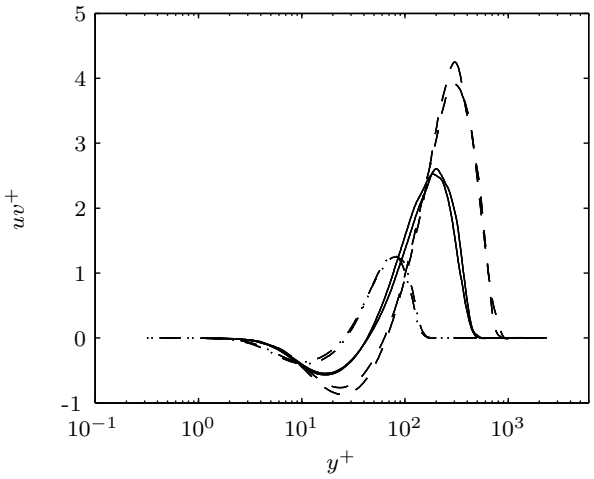

Figure 9: Reynolds stress, in inner scaling, at downstream positions $x/h = 20$ and 25. Isothermal (solid), warm (dashed) and cold jet (dash-dotted) results.

outer flow scale ratio, is such that the friction Reynolds numbers, using the using the maximum streamwise position as characteristic outer length scale is; $Re_{\tau,c} < Re_{\tau,i} < Re_{\tau,w}$. Correspondingly, in the warm jet smaller turbulent structures are present than in the cold jet. The wall-jet growth rate is highest in the cold jet and lowest in the warm jet, which corresponds to what have been found in previous wall-jet investigations for increasing inlet Reynolds number. When using viscous scaling, the differences in turbulent properties in the inner and outer parts of the jet are pronounced in the warm jet, and the scaled turbulent kinetic energy and Reynolds stress magnitudes increase. The opposite occur for the cold jet statistics. The differences in density also influences the temperature and passive scalar fluctuations. The difference in the temperature fluctuation intensity between the inner and outer shear layers becomes less pronounced in the warm jet than in the cold jet. The passive scalar fluctuation intensity is approximately equal in the three jets in the near wall region, further out the warm jet fluctuation increases further, while the isothermal and

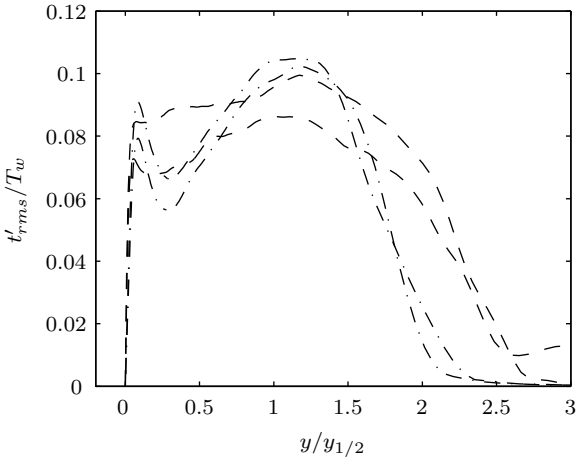

Figure 10: Temperature fluctuation intensities, scaled by the wall temperature, at downstream positions $x/h = 20$ and 25. Warm (dashed) and cold jet (dash-dotted) results.

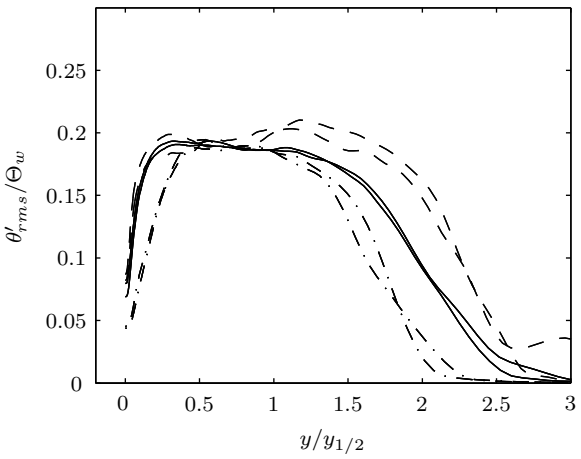

Figure 11: Passive scalar fluctuation intensities, scaled by the mean wall concentration, at downstream positions of $x/h = 20$ and 25. Isothermal (solid), warm (dashed) and cold jet (dash-dotted) results.

cold jet fluctuation decreases monotonically.

ACKNOWLEDGEMENTS

Funding for the present work has been provided by the The Centre for Combustion Science and Technology (CECOST). The computations were performed at the Center for Parallel Computers at KTH, using time granted by the Swedish National Infrastructure for Computing (SNIC). Prof. Bendiks Jan Boersma is thanked for providing the original version of the DNS code.

REFERENCES

Abrahamsson, H., Johansson, B., and Löfdahl, L., 1994, "A turbulent plane two-dimensional wall-jet in a quiescent surrounding," *Eur. J. Mech. B/Fluids*, Vol. 13, pp. 533-556.

del Álamo, J. C., Jiménez, J., Zandonade, P., and Moser, R. D., 2006 "Self-similar vortex clusters in the turbulent logarithmic region," *J. Fluid Mech.*, Vol 561, pp. 329-358.

Ahlman D., Brethouwer, G., and Johansson A. V., 2007, "Direct numerical simulation of a plane turbulent wall-jet including scalar mixing", *To appear in Phys. Fluids.*

Antoine, Y., Lemoine, F., and Lebouché, M., 2001, "Turbulent transport of a passive scalar in a round jet discharging into a co-flowing stream", *Eur. J. Mech. B - Fluids*, Vol. 20, pp. 275-301.

Dejoan A., and Leschziner, M. A., 2005 "Large eddy simulation of a plane turbulent wall jet", *Phys. Fluids*, Vol. 17, pp. 025102.

Dejoan A., and Leschziner, M. A., 2006 "Separating the effects of wall blocking and near-wall shear in the interaction between the wall and the free shear layer in a wall jet", *Phys. Fluids*, Vol. 18, pp. 065110.

Eriksson J. G., Karlsson R. I., and Persson J., 1998, "An experimental study of a two-dimensional plane turbulent wall jet", *Experiments in Fluids*, Vol 25, pp. 50-60.

Freund, J. B, 1997 "Proposed inflow/outflow boundary condition for direct numerical computation of aerodynamic sound", *AIAA Journal*, Vol 35 (4), pp. 740-742.

Fulachier, L., Borghi, R., Anselmet, F., and Paranthoen, P., 1989, "Influence of density variations on the structure of low-speed turbulent flows: a report on Euromech 237", *J. Fluid Mech.*, Vol. 203, pp. 577-593.

Huang, P. G., Coleman, G. N., and Bradshaw, P., 1995, "Compressible turbulent channel flows: DNS results and modelling", *J. Fluid Mech.*, Vol. 305, pp. 185-218.

Launder, B. E., and Rodi W., 1981, "The turbulent wall jet", *Prog. Aerospace Sci.* Vol. 19, pp. 81-124.

Launder, B. E., and Rodi W., 1983 "The turbulent wall jet – measurements and modelling", *Ann. Rev. Fluid Mech.* Vol. 15, pp. 429-459.

Lele S. K., 1992, "Compact finite difference schemes with spectral-like resolution", *J. Comp. Phys.*, Vol 103, pp. 16-42.

Levin O., Chernoray, V. G., Löfdahl, L., and Henningson, D. S., 2005 "A study of the blasius wall jet", *J. Fluid Mech.*, Vol 539, pp. 313-347.

Österlund, J. M., 1999, "Experimental studies of zero pressure-gradient turbulent boundary layer flow", Ph.D. Thesis, Royal Institute of Technology, Stockholm, Sweden

Österlund, J. M., Johansson A. V., Nagib H. M., Hites M. H., 2000 "A note on the overlap region in turbulent boundary layers", *Phys. Fluids*, Vol. 12, pp. 1-4.

Stanley, S. A., Sarkar, S., and Mellado, J. P., 2002, "A study of the flow-field evolution and mixing in a planar turbulent jet using direct numerical simulation", *J. Fluid Mech.*, Vol. 450, pp. 377-407.

Su, L. K., and Clemens, N. T., 2003, "The structure of fine-scale scalar mixing in gas-phase planar turbulent jets", *J. Fluid Mech.*, Vol. 488, pp. 1-29